Zebrafish xenograft model: Identification of novel mechanisms driving prostate cancer metastasis

Chen, L.

Chapter 3

Zebrafish microenvironment elevates EMT and CSC-like phenotype of engrafted prostate cancer cells

Lanpeng Chen[1], Maciej Boleslaw Olszewski[2,3], Marianna Kruithof-de Julio[4,5] and B. Ewa Snaar-Jagalska[1*]

[1]Institute of Biology, Leiden University, Leiden, Netherlands

[2]Department of Molecular Biology, International Institute of Molecular and Cell Biology, Warsaw, Poland

[3]Center for Biomedical Research, Faculty of Veterinary Medicine, Warsaw University of Life Sciences, Warsaw, Poland

[4] Department for BioMedical Research, Bern University, Bern, Switzerland

[5]Department of Urology, Inselspital, Bern , Switzerland

*Corresponding author

Prof. B. Ewa Snaar-Jagalska, b.e.snaar-jagalska@biology.leidenuniv.nl

Cells, 2020, 9(4), 797.

Abstract

To visually and genetically trace single cell dynamics of human prostate cancer (PCa) cells at the early stage of metastasis, a zebrafish (ZF) xenograft model was employed. The phenotypes of intravenously transplanted fluorescent cells were monitored by high-resolution, single cell intravital confocal and light-sheet imaging. Engrafted osteotropic, androgen independent PCa cells extravasated from caudle vein, invaded the neighboring tissue, proliferated and formed experimental metastasis around caudal hematopoietic tissue (CHT) in four days. Gene expression comparison between cells in culture and in CHT revealed that engrafted PCa cells responded to the ZF microenvironment by elevating expression of EMT and stemness makers. Next, metastatic potential of $ALDH^{hi}$, cancer stem-like cells (CSCs) and $ALDH^{low}$ non-CSCs was analyzed in ZF. Engraftment of CSCs induced faster metastatic onset, however after four days both cell subpopulations equally responded to ZF microenvironment, resulting in the same increase of stemness genes expression, including Nanog, Oct-4 and Cripto. Knockdown of Cripto significantly reduced Vimentin/E-Cadherin ratio in engrafted cells, indicating that Cripto is required for transduction of the microenvironment signals from the ZF niche to increase mesenchymal potential of cells. Targeting of either Cripto or EMT transcriptional factors Snail 1 and Zeb1 significantly suppressed metastatic growth. This data indicated that zebrafish microenvironment governed CSC/EMT plasticity of human PCa cells, required for metastasis initiation.

Introduction

Prostate cancer (PCa) is one of the most prevalent cancer disease in men around the world [1]. 20-30% of the patients who originally respond to initial treatments can still develop androgen independent and treatment-resistant bone metastasis, which is the main cause of death. Metastasis is a complex, multiple-steps process led by intravasation of single cancer cells/clusters into vasculature from the primary site [2]. After circulating in blood flow and extravasation, only very few cancer cells that have homed and responded to foreign microenvironment can eventually develop metastatic tumor growth [3]. More recently, a small subpopulation of the cancer cells called cancer stem-like cells (CSCs) are indicated to initiate PCa bone metastasis [4, 5]. Those cells are characterized by high self-renewal capacity, tumorigenicity and chemoresistance. A number of proteins are identified as PCa CSC markers including CD44, integrin α2β1 and ALDH1A1 [6, 7]. Moreover, cell subpopulation with high Aldehydedehydrogenase (ALDH) activity has been reported as CSC-enriched subpopulation and characterized by high expression of CD44, integrin α2β1, enhanced clonogenicity in vitro, and metastatic capacity in vivo [7]. Hence, targeting of this cell subpopulation may have a positive clinical outcome. Importantly, it is suggested that CSCs can be dedifferentiated from non-CSCs in multiple types of cancer including PCa [8-10]. This so-called cancer CSC-plasticity is hypothetically driven by the molecular and cellular cues present in tumor microenvironment [3, 8]. Understanding of the underlying mechanisms driving cancer plasticity is therefore essential for anti-CSC drug development.

The emergence of CSCs are closely linked to epithelial-mesenchymal transition (EMT) [11-13], a developmental program promoting cancer progression [14-16]. Once happens, cancer cells lose cell-cell junction and gain motility inducing metastatic dissemination [14]. Multiple studies have indicated that the production of CSCs is partially a result of EMT [11, 17]. Transient expression of EMT transcriptional factors Snail1 can induce tumor recurrence and metastasis [18, 19]. In addition, EMT is a highly plastic process. Cancer cells can shift between EMT and its reversed program, MET, at different steps of metastatic cascades, endowing the cells with distinct properties like migration, invasion, quiescence, and re-entry of tumor growth [20]. However, due to a lack of tools to detect single cell status at each steps of the metastatic cascades, the precise roles of EMT and MET in the whole metastatic process are still controversial [21].

Zebrafish (ZF) has been employed as a powerful platform for cancer research due to its high genomic conservation with human [22-24]. It is widely conducted to model the initiation and malignant progression of different types of cancer [22, 25, 26]. ZF xenograft models with different human cancer cells have been established [24, 27]. Due to an absence of mature adaptive immunity at the embryonic stage, human cancer cell lines and patient-derived primary cancer cells can survive, grow and metastasize in ZF [25]. The optical transparency of the embryo enables imaging of all steps of cancer progression at a single cell resolution in live animal. The high molecular similarity between human and ZF permits the human cancer cells to sense and respond to ZF microenvironment cues during cancer progression [28, 29]. High throughput screens can be easily performed to assess the metastatic capacity of different cancer cells and to test their therapeutic responses to drugs [26].

To visually and genetically trace PCa cell plasticity at the early stagy of metastasis, fluorescence labeled PCa cells were intravenously injected into zebrafish, inducing formation of metastatic lesion at the zebrafish hematopoietic tissue. Immunofluorescence and RT-PCR analysis revealed an induction of EMT, enrichment of $ALDH^{hi}$ CSC subpopulation and upregulation of CSC markers when the PCa cells colonized the metastatic site. We previously reported that Cripto is a stemness gene that governs PCa metastasis in zebrafish and mice xenografts [34]. Furthermore, we observed that co-culturing of PCa cells with osteoblast induced Cripto expression, suggesting possible involvement of bone niche signals in its regulation [34]. Here, we showed that the expression of Cripto in the engrafted cells was upregulated by ZF microenvironment. This microenvironment-induced Cripto drove experimental metastatic colonization through induction of EMT plasticity. Targeting of either Cripto or EMT transcriptional factors significantly inhibited metastatic growth. Altogether, our data indicated that human PCa cells can respond to the zebrafish molecular and cellular cues inducing Cripto-mediated EMT/CSC plasticity, which leads to metastatic tumor initiation.

Materials and Methods

Cell culture

Human embryonic kidney cells HEK-293T (kindly provided by Dr. Sylvia Le Dévédec, LACDR, Leiden) were maintained in DMEM supplemented with 10% FCS. Human PCa cell line PC-3-mCherry was maintained in Nutrient Mixture F-12K supplemented with 10% FCS while PC-3M-Pro4-mCherry (kindly provided by Dr. Gabriel van der Pluijm, Department of Urology, LUMC) was DMEM supplemented with 10% FCII (Hyclone™).

Zebrafish maintenance, tumor cell implantation and metastasis analysis

Wildtype zebrafish (ZF) line ABTL and transgenic line tg (Fli:GFP) [30] were handled in compliance with local animal welfare regulations and maintained according to standard protocols (www.ZFIN.org).

Cancer cell transplantation was performed as described before [27]. In brief, at two days post-fertilization (dpf), dechorionated ZF embryos were anaesthetized with 0.003% tricaine (Sigma) and plated on a Petri dish covered with 1.5% of solidified agarose. Cancer cells were trypsinized, suspended in PBS containing 2% polyvinylpyrrolidone (PVP; Sigma-Aldrich) with a concentration of 200,000 cells/ul and loaded in into borosilicate glass capillary needles (1 mm O.D. × 0.78 mm I.D.; Harvard Apparatus). 300-500 cancer cells were injected into duct of cuvier (DoC) of ZF embryos using a Pneumatic Picopump and a manipulator (WPI). The injected embryos were further maintained in a 34 ˚C incubator. Images were acquired with a Leica M165 FC stereo fluorescent microscope at 1-, 2-, 4- and/or 6- days post injection (dpi). Data was further analyzed with image J software and/or ZF4 pixel counting program (Leiden). For high resolution imaging, zebrafish embryos were placed on glass-bottom petri dishes and covered with 1% low melting agarose containing 0.003% tricaine (Sigma). Images were acquired using a Leica SP8 confocal microscope (Leica) or Nikon Eclipse Ti confocal laser-scanning microscope (Nikon) and processed with image J software.For light-sheet microscopy zebrafish embryos were anesthetized with 0.003% tricaine, embedded in 1% low melting agarose with tricaine and mounted in Zeiss light-sheet Z.1 capillary specimen holder, vertically immersed in imaging chamber containing water with tricaine. For whole-trunk imaging (Fig. 1b) and for single-cell imaging (Fig. 1c) 20x and 40x objectives were used, respectively. Specimens were imaged in single-track dual-channel mode to minimize spatial shift between channels. For each area 4 stacks were acquired with specimen axial rotation of 90° between stacks. Specimen 3D structure was reconstructed using multiview fusion and deconvolution (Zeiss ZEN software). Surface rendering was performed using Imaris 8.1 with solid or semitransparent vasculature, to aid observation of both intra- and extravascular cells.

Immunofluorescence

Whole mount immunofluorescence on ZF was performed as described before [31]. ZF was fixed with 4% PFA, dehydrated and rehydrated with methanol in series concentration (25%,

50%, 75% and 100%). After permeabilization with 10ug/ml Protease K, embryos were blocked using blocking buffer containing 0.7%Triton X-100 and 5% sheep serum in 0.5% PBST. After incubation with primary (1/200) and fluorescence-conjugated secondary (1/200) antibodies, images were acquired using Leica SP8 confocal laser-scanning microscope.

ALDEFLUOR assay and FACS sorting

Cancer cells with high Aldehyde dehydrogenase (ALDH) activity were detected and sorted using ALDEFLUOR Assay kit (StemCell technology) following the manufacturer's protocol. Briefly, 1-10 million PC-3M-Pro4-mCherry cells were treated with the ALDEFLUOR reagent. To set the gate for negative population, 500.000 PC-3M-Pro4-mCherry cells were treated with ALDEFLUOR reagent together with DEAB, an ALDH inhibitor. FACSCanto II (BD Biosciences) was used for the measurement and data was further analyzed with FCS Express Software (De Novo Software). Each condition was independently repeated 3 times. For whole mount ALDFLJUOR live staining on ZF, 6 dpf ZF was embedded in 1% low melting temperature agrose. 10x concentrated ALDEFLUOR reagent in ALDEFLUOR buffer was dropped on ZF. After incubation at 34°C for 1 hour, ZF was immediately imaged using Leica SP8 confocal laser-scanning microscope.

RNA extraction and qPCR

Total RNA isolation from ZF was performed as described before [31]. Metastasis samples in ZF were collected by cutting the whole metastatic site (80 fish per group) at 6dpi using a micro dissection scissor (WPI). After cutting, the samples were immediately washed with cold PBS and stored in TRIzol (Sigma) at -20 ˚C. The whole process was finished within 30 min. Whole RNA was isolated using the RNeasy mini kit (qiagen) following the manufacturer's protocol. iScript™ cDNA Synthesis Kit (Bio-Rad) was used for cDNA synthesis and iQ™ SYBR® Green Supermix (Bio-Rad) was for qPCR as described in the manufacture's protocol. For each gene analysis, human specific primers were designed in order to measure the gene expression variation in human cancer cells. The species-specificity was tested before the experiments. GAPDH was included as housekeeping for normalization. Three independent experiments were performed.

Lentivirus production and transduction

Short hairpin RNA (shRNA) constructs against Cripto-1, Snail1 and Zeb1 were obtained from Sigma's MISSION library (Kindly provided by Department of Molecular Cell Biology, LUMC). Lentivirus were produced by transforming pLenti constructs, packaging plasmids psPAX2 and enveloped plasmids pMD2.G (Addgene plasmid) into HEK-293T cells using lipoD293 (SignaGen Laboratories) as transforming reagent. Lentivirus supernatant was collected at 72hour after transformation. Cells were transduced with the lentiviruses using 6ug/ml Polybrene (Sigma-Aldrich).

Statistics

Statistics analysis was performed with Graphpad Prism 7.0 (San Diego, CA, USA). t-Test was used to compare two groups and ANOVA for multiple groups. Data is presented as mean ±SEM or mean ±SD. p-values ≤0.05 are considered to be statistically significant (*p≤0.05, **p<0.01, ***p<0.001, ****P<0.0001)

Results

Intravenous transplantation of PCa cancer cells into zebrafish leads to development of extravascular metastatic tumor growth

Androgen independent osteotropic PC-3M-Pro4-mCherry cells (100-400 cells) were intravenously injected into duct of cuvier (DoC) of tg(Fli:GFP) endothelial reporter transgenic zebrafish line with fluorescent vasculature (REF) at 2 days post fertilization (dpf) (Fig. 1a). DoC is an open blood circulation channel connecting the heart and the trunk vasculature. Immediately after transplantation cells haematogenously disseminated through whole circulation. Most of the circulating cells regressed without extravasation and initiating tumor growth. However, exclusively at the posterior ventral end of caudal hematopoietic tissue (CHT) perivascular cells were able to extravasate and invade into tail fin within 1 day and developed perivascular metastatic lesions within 6 days (Fig. 1a, 1b). CHT is a ZF hematopoietic organ at early developmental stage with a certain molecular and cellular similarity to mice bone marrow [29, 32]. To image cellular details of the metastatic phenotype, at 6 days post injection (dpi), high-resolution imaging was performed using Light-sheet Confocal microscope (Fig. 1b, 1c). This image proved that single cancer cells circulated in the blood flow and extravasated from intersegmental vessel (ISV), dorsal longitudinal anastomotic vessel (DLV), Dorsal vein (DA) and caudal vein (CV) (Fig. 1c). The metastatic tumor growth around CHT was characterized using immunofluorescence. Abundant phosphorylated-Histone3 positive cells were detected (Fig. 1d), indicating that expended red fluorescent signal is indeed due to proliferation of PCa cells at metastatic site. This novel experimental metastatic assay bypasses the primary tumor stage and intravasation but opens possibility to image and study the mechanisms controlling metastatic initiation of PCa cells in a few days, instead of weeks in rodent models.

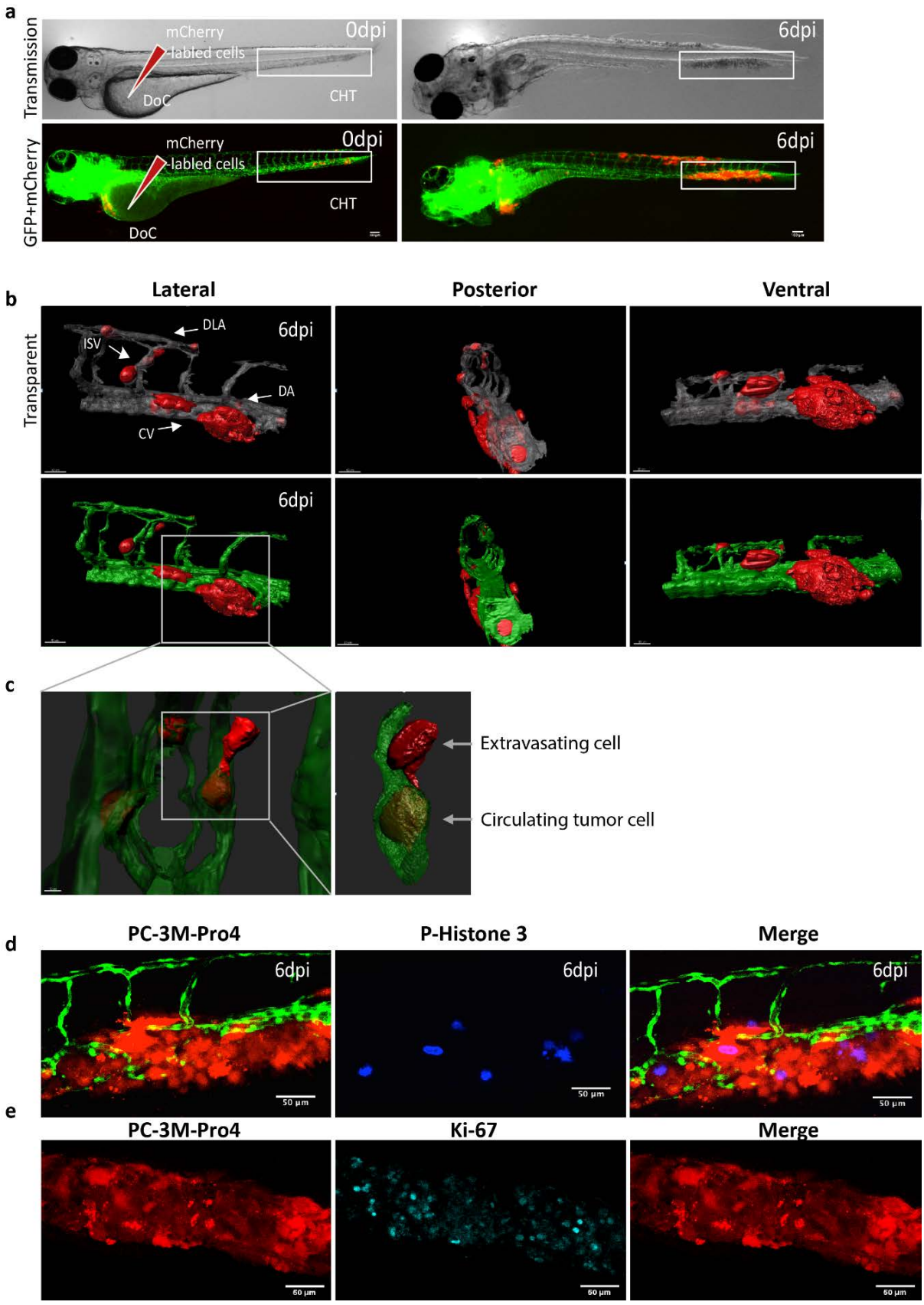

Figure. 1 Intravenous transplantation of PCa cells induces extravasation and perivascular metastasis formation. (a) Schematic indication of cancer cell engraftment. PC-3M-Pro4-mCherry was injected into ZF vasculature. Metastases was formed at 6dpi. Red, cancer cells. Green, vessels. (b-c) High resolution images were acquired using a Light-sheet microscope. Scale bar=100 um. (b) 3-dimensional overview of metastatic phenotype of the

cancer cells at 6dpi. Left, lateral. Middle, posterior. Right, Ventral. Up, solid vessels. Down, transparent vessels. Imaging was acquired using Zeiss Lightsheet Z1 at 40x magnification. Zeiss ZEN software was used for multiview fusion and deconvolution. Image J and Imaris 8.1 were applied for imaging stitching and 3D rendering. (c) High magnification images to show single cell behaviors. Single cells extravasated from intersegmental vessel (ISV), dorsal longitudinal anastomotic vessel (DLV) and Dorsal vein (DA). Up, solid vessels. Down, transparent vessels. (d-e) Whole mount immunofluorescence against phosphorylated Histone 3 (d) and Ki-67 (e) at 6 dpi. Images were acquired using confocal. Scare bar=50um.

Oesteotropic PCa cells with enhanced EMT and CSC traits have stronger metastatic potential in ZF

To prove usefulness of ZF model, we compared the metastatic capacity of two PCa cell lines: PC-3 and PC-3M-Pro4. PC-3M-Pro4 is a metastatic subclone of PC-3, derived by 4 times orthotropic transplantation of PC-3 into mice prostate, endowing the cells with a strong bone metastatic potential in mice [33]. After intravascular injection into ZF embryos, PC-3 cells were circulating in blood flow at 1- and 2-days post injection (dpi) (Fig. 2a). At 4 dpi, majority of the cells were cleared however a few cells survived and extravasated into the neighboring tissue around CHT (Fig. 2a). In contrast, PC-3M-Pro4 cells docked at CHT at 1dpi, extravasated and formed experimental metastasis at 4dpi (Fig. 2a). Extravasation of PC-3 and PC-3M-Pro4 were evaluated by counting the percentage of ZF with more than one cell extravasated from caudle vein and invaded the neighboring tissue (Fig. 2a, Fig. 2b). PC-3 extravasated only in 5% of the engrafted ZF at 1 dpi, 10% at 2dpi and 20% at 4dpi but PC-3M-Pro4 extravasated in 10% at 1dpi and 50% at 2 and 4dpi (Fig. 2b). Metastatic tumor outgrowth was determined by measuring total fluorescence intensity in the trunk and CHT (Fig. 2c). Total cancer cell burden of PC-3 at the metastatic site decreased following the time while the cancer cell burden of PC-3M-Pro4 was gradually increasing and was significantly higher at 2 and 4 dpi then PC-3 (Fig. 2c).

Next, we questioned why PC-3M-Pro4 had stronger metastatic potential than PC-3. Gene signatures for EMT and cancer stemness were analyzed using qPCR. PC-3M-Pro4 cells in culture had elevated expression of mesenchymal markers N-Cadherin, Vimentin, twist, zeb1 and snail1, and stemness markers Nanog, Sox2 and Bmi-1 (Fig 2d, 2e). Notably, PC-3M-Pro4 also exhibited a higher expression of epithelial marker E-Cadherin, indicating these cells had a trait of partial EMT rather than fully EMT where the expression of E-Cadherin is missing. Those data suggest that, enhanced metastatic capacity of PC-3M-Pro4 in zebrafish and mice models relies on the elevated expression of stemness and EMT genes.

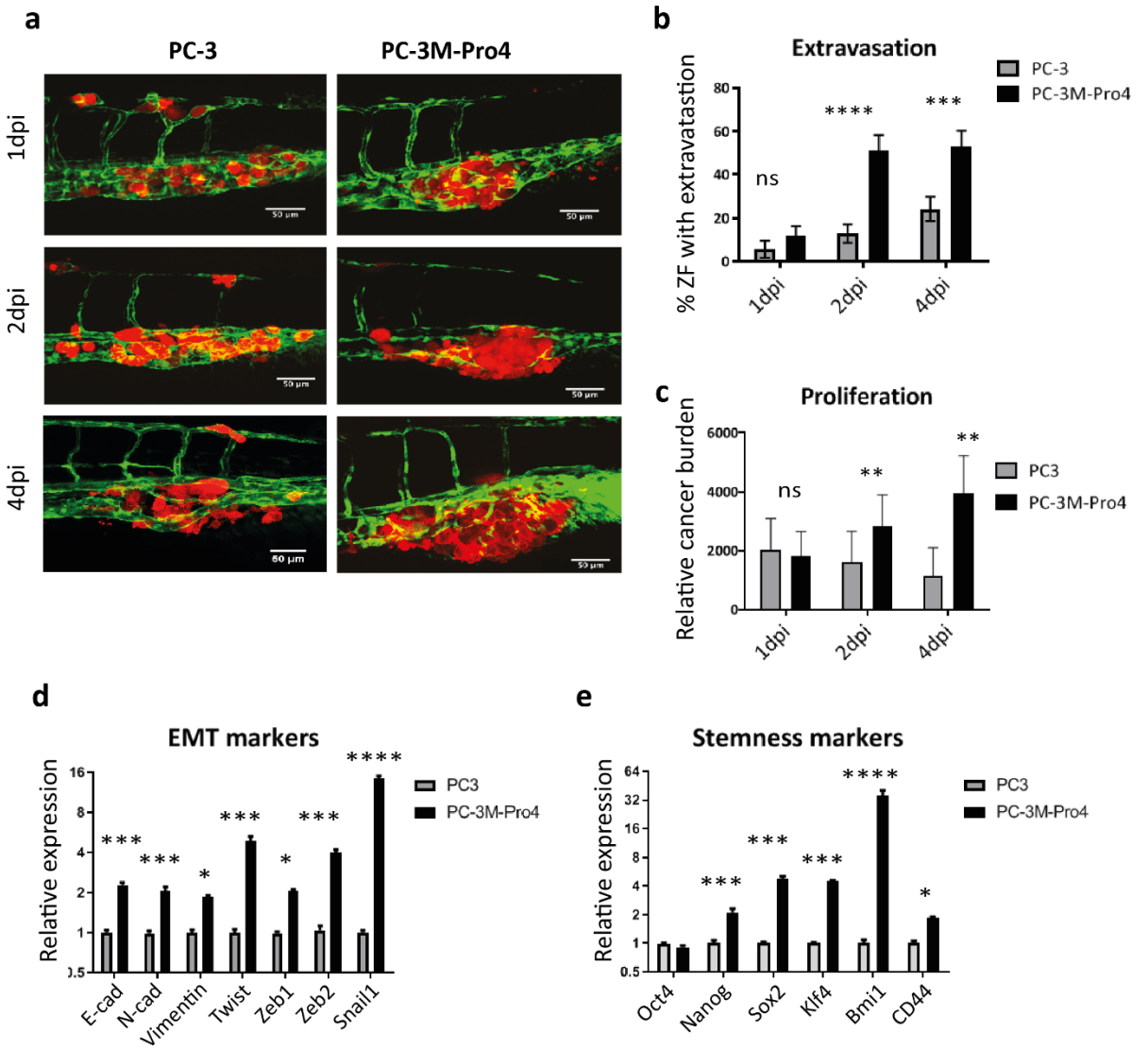

Figure 2. PC-3M-Pro4 with enhanced EMT and CSC traits in comparison with PC-3 have stronger extravasation and metastatic tumor-initiating capacity. (a) PC-3-mCherry and PC-3M-Pro4-mCherry were injected into ZF vasculature. Confocal images were acquired at the metastatic site at 1, 2 and 4dpi. Green, vessels. Red, cancer cells. Scale bar=50um. (b-c) Extravasation and cancer cell burden at the metastatic site were analyzed. For extravasation analysis, % of ZF with more than 1 cells extravasated from the caudal vein and invaded into neighboring tissue was counted. For cancer cell burden quantification, total fluorescence of mCherry was measured using a ZF-4 pixel counting software. Group size=60. (d-e) The expression of EMT markers and Stemness markers in PC-3 and PC-3M-Pro4 in culture was measured by qPCR. Group size=3.

Metastatic outgrowth of PCa cells in ZF is associated with an increase of EMT and cancer stemness markers

We next measured how human cancer cells responded to the ZF microenvironment during the formation of metastatic lesions at the CHT area. At 6dpi, RNA samples were collected from the metastatic lesions formed by PC-3M-Pro4 in 210 ZF embryos (Fig. 3a). QPCR was performed using human specific primers without cross reactivity with ZF tissue to compare gene expression profiles of the cancer cells in metastases and in cells culture. Consequently, the cancer cells from metastasis exhibited a significantly enhanced expression of

mesenchymal marker Vimentin, twist and zeb2 and a decrease of epithelial marker E-Cadherin (Fig. 3b). Moreover, these cells also gained expression of stemness genes including Nanog, Oct4, ALDH7A1 and Cripto (Fig. 3c).

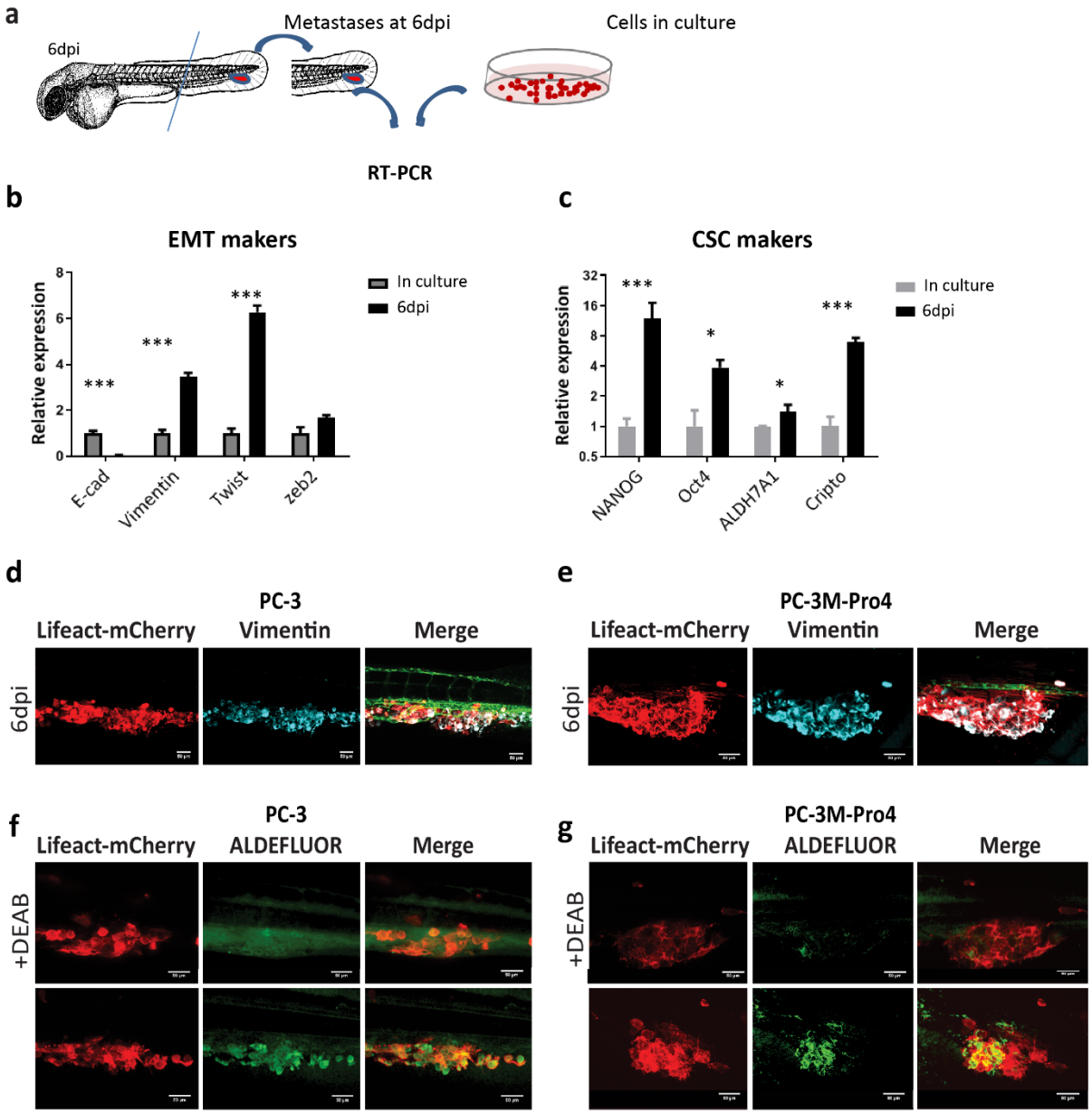

Figure. 3 PCa cells obtain enhanced EMT and CSC traits after colonizing ZF CHT area. (a) Schematic indication of RNA isolation from ZF metastases. At 6dpi, ZF tails containing metastatic lesions were cut and collected for RNA isolation. (b-c) The expression of EMT markers and Stemness markers were compared between in culture and in ZF metastases at 6dpi. Group size=3. (d-e) Immunofluorescence against Vimentin on PC-3 and PC-3M-Pro4 in ZF metastases. (f-g) ZF engrafted with PC-3 and PC-3M-Pro4 was stained with ALDEFLUOR reagent with or without ALDH inhibitor DEAB. Images were acquired using SP-8 confocal and processed with Fiji. Scale bar=50um. Group size=5.

In addition, whole mount immunofluorescence against vimentin was performed on PC-3 and PC-3M-Pro4 to further examine the EMT features. In vitro, all PC-3M-Pro4 cells had Vimentin expression but only very few elongated cells in PC-3 expressed vimentin (data not shown). After colonizing ZF CHT at 6dpi, however, both PC-3 and PC-3M-Pro4 displayed extensive and homogeneous expression of Vimentin, indicating an acquisition of EMT feature during the metastatic process (Fig. 3d, 3e).

Given that the cancer cell subpopulation with high Aldehydedehydrogenase activity is identified in vitro as a CSC-enriched cell subpopulation, we applied ALDEFLUOR assay to measure the CSC features of cells at metastatic site. At 4dpi, live ZF engrafted with either PC-3 and PC-3M-Pro4 were stained with ALDEFLUOR reagent, a fluorescence dye labelling viable $ALDH^{hi}$ cells. To set the negative control, some of the engrafted ZF were treated with the ALDH inhibitor DEAB when exposing to ALDEFLUOR reagent. Although no or very few ALDH signals were detected in the DEAB treated ZF (Fig. 3f, 3g), in DEAB untreated ZF, both PC-3 and PC-3M-Pro4 exhibited strong ALDH signals at the metastatic site (Fig. 3f, 3g). Altogether, our data reveal that both PCa cell linesrespond to the ZF microenvironment factors resulting in an enhancement of EMT and CSC markers leading to metastatic tumor initiation.

Both $ALDH^{hi}$ and $ALDH^{low}$ cells obtain an enhanced CSC trait after metastatic colonization

Subsequently, we compared the metastatic potential of PCa CSCs and non-CSCs sorted by ALDEFLUOR assay from PC-3M-Pro4 (Fig. 4a). The aggressiveness of the cells was firstly tested in vitro. 3D invasion assay was employed by embedding 500 cells into type-I collagen and size of the invasion area was measured after 72 hours. In comparison with the $ALDH^{low}$ cell, the $ALDH^{hi}$ cells had a significantly enhanced invasive phenotype. (Fig. 4b). Clonogenicity assay was employed to compare self-renewal capacity of the cells by seeding 200 single cells into 6 wells plate. After 14 days of growth, significantly more colonies were formed by $ALDH^{hi}$ cells (Fig. 4c). Collectively, those *in vitro* data indicate that the $ALDH^{hi}$ cells are more invasive and proliferative *in vitro* than its $ALDH^{low}$ counterpart.

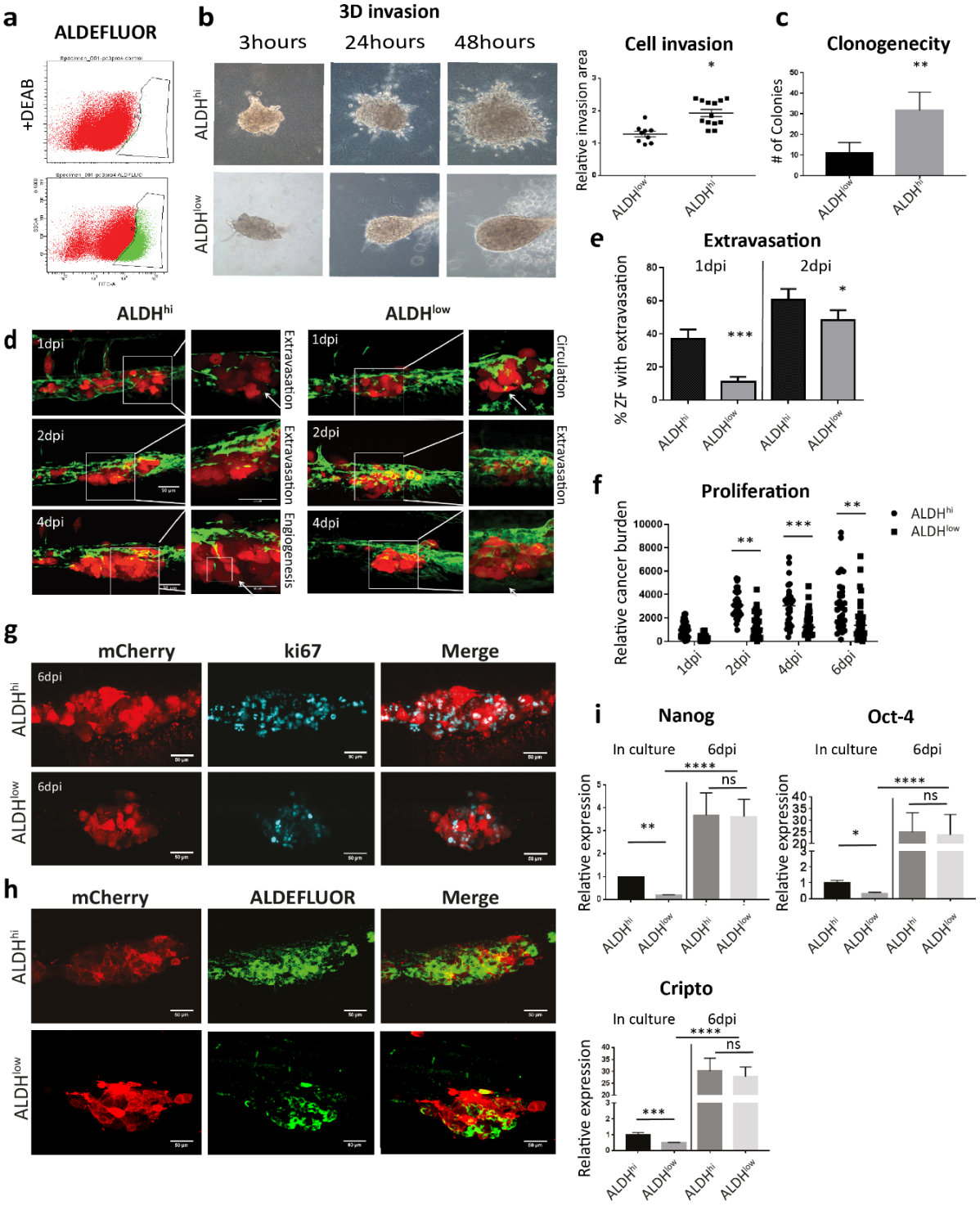

Figure. 4 Both ALDHhi and ALDHlow cell subpopulation obtain enhanced CSC traits after colonizing ZF CHT area. (a) Gate setting for ALDHhi and ALDHlow cell sorting. (b) After sorting, both ALDHhi and ALDHlow subpopulation were respectively injected into type I collagen. Cell invasion was quantified by measuring the fold change of the invasive area after 48 hours. Group size=10. (c) ALDHhi and ALDHlow cells were seed for Clonogenicity. Number of colonies formed by the cells was counted after 14days of culture. (D) ALDHhi and ALDHlow cells were injected into ZF after sorting. Confocal images were acquired at 1, 2, 4 and 6dpi. Scale bar=50um. Green, vessel. Red, cancer cells. Left, 20X magnification. Right, 63X magnification. (e-f) Extravasation and cancer cell burden at the metastatic site were analyzed. Group size =30. (g-h) Immunofluorescence against ki-67 and ALDEFLUOR staining were performed on engrafted ZF. Confocal images were acquired at the metastatic site. Scale bar=50um. (i)

Expression of stemness genes in ALDHhi and ALDHlow was measured by qPCR in the cells after sorting and in the ZF metastases at 6dpi.

We next analyzed the aggressive phenotype of $ALDH^{hi}$ and $ALDH^{low}$ cell subpopulations sorted from PC-3M-Pro4-mCherry in ZF xenografts. After engraftment, the $ALDH^{hi}$ cells extravasated and invaded in 40% of the engrafted ZF at 1dpi while $ALDH^{low}$ extravasated only in 10% of embryos (Fig. 4d, 4e). At 2dpi, the difference of extravasation between two cell types was smaller but still significant (Fig. 4d, 4e). In addition, cancer cell burden at the metastatic site was measured. $ALDH^{hi}$ cells had significantly higher cancer cell burden than $ALDH^{low}$ (Fig. 4f). Notably, at 6dpi, some of the fish engrafted with $ALDH^{low}$ still developed metastatic tumor growth however significantly lower comparing to ALDHhi (Fig. 4f). We showed by immunofluorescence that the metastases formed by both cell subpopulations were rapidly growing since numerous Ki-67 (proliferation marker) positive cells were detected in both $ALDH^{hi}$ and $ALDH^{low}$ cells (Fig. 4g).

To assess if ZF microenvironment can regulate the stemness phenotype of the $ALDH^{hi}$ and/or $ALDH^{low}$ cells, ZF engrafted with either $ALDH^{hi}$ or $ALDH^{low}$ were stained with ALDFLUOR reagent at 4dpi. Although extensive ALDEFLUOR signal was detected in the metastases formed by $ALDH^{hi}$ cells (Fig. 4h), some of the $ALDH^{low}$ cells also displayed the positive ALDEFLUOR signal, indicating a re-enrichment of $ALDH^{hi}$ subpopulation in the engrafted $ALDH^{low}$ cells during metastatic colonization (Fig. 4h).

Furthermore, we compared the expression of stemness genes in two cell subtypes directly after cell sorting and in metastatic lesions. Before injection, the $ALDH^{hi}$ cells displayed enhanced expression of stemness markers Nanog, Oct4 and Cripto-1 than the $ALDH^{low}$. Surprisingly, at 6 dpi after engraftment to ZF, the expression of Nanog, Oct4 and Cripto was significantly increased to a similar level in both cell subtypes (Fig. 4i). Taken together, our results indicate that both $ALDH^{hi}$ and $ALDH^{low}$ cells can respond to the microenvironment in ZF, inducing an augment of stemness feature.

Knockdown of Cripto inhibited PCa cell metastatic tumorigenicity through suppressing EMT-plasticity

The Nodal signaling co-receptor Cripto has been well documented to play an essential role in maintaining stemness in both embryonic stem cells and CSCs. In PCa, high expression of Cripto correlates with poor prognosis and high risk of metastasis in the patients [34]. We have previously showed that Cripto had higher expression in $ALDH^{hi}$ subpopulation. The knockdown of Cripto using shRNA significantly inhibited the size of $ALDH^{hi}$ fraction in vitro and metastasis in ZF at 4dpi and mice at 5 weeks after injection, respectively [34]. Here, we further investigated if microenvironment-induced Cripto was required for the cancer cell plasticity during metastasis (Fig. 4i). To test this PC-3M-Pro4 cells bearing either SCR or Cripto kd were engrafted into ZF. As expected, metastatic growth was significantly suppressed by Cripto kd at 6dpi (Fig. 5a). We collected the metastases tissue and performed cross-species RT-PCR using specific primers (Fig. 5b). The knockdown of Cripto significantly reduced Vimentin/E-Cadherin

ratio in vivo, indicating that elevation of Cripto expression in engrafted cells by factors from metastatic niche was indeed required for the acquisition of EMT trait during the metastatic colonization (Fig. 5b).

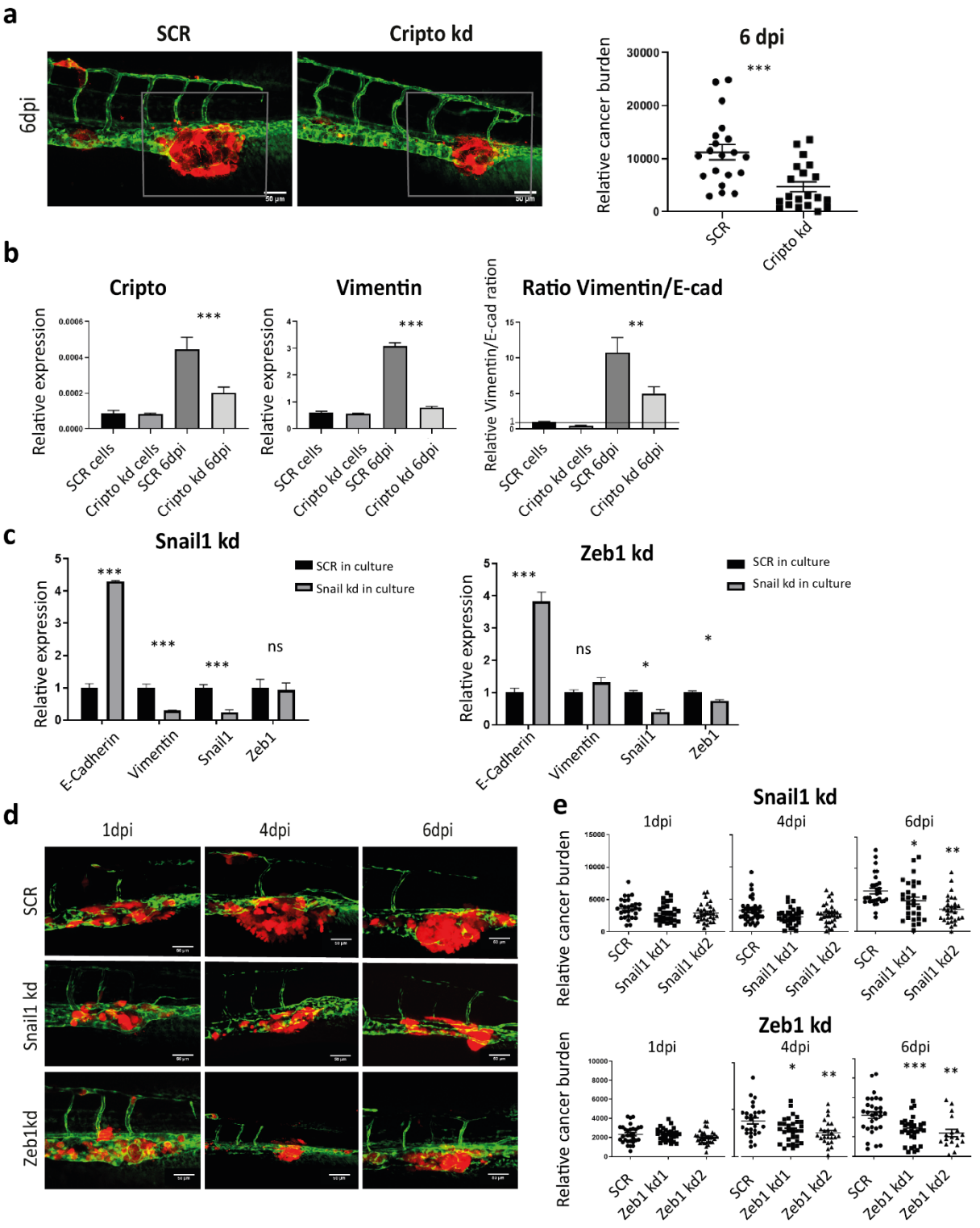

Figure. 5 Cripto drives metastatic phenotype through controlling EMT plasticity. (a) PC-3M-Pro4-mCherry-SCR and PC-3M-Pro4-mCherry Cripto kd were injected into ZF. Confocal images were acquired at 6dpi. Green, vessels. Red, cancer cells. Scale bar=50um. Cancer cell burden at the metastatic site was quantified by measuring total

fluorescence intensity at 6dpi. Group=30. (b) Cancer cell burden at the metastatic site was quantified by measuring total fluorescence intensity. Group size=30. (c) Expression of Cripto, stemness markers and EMT markers was measured in PC-3M-Pro4-mCherry-SCR and PC-3M-Pro4-mCherry-Cripto kd in culture and in ZF metastases at 6dpi. Group size=3. (d) Expression of EMT markers was compared between PC-3M-Pro4-mCherry-SCR, -Snail1 kd and -Zeb1 kd. Group size=3. (e) PC-3M-Pro4-mCherry-SCR, -Snail1 kd and -Zeb1 kd were injected into ZF. Confocal images were acquired at 1, 4 and 6 dpi. Green, vessels. Red, cancer cells. Scale bar=50um. (f) Cancer cell burden at the metastatic site was quantified by measuring total fluorescence intensity. Group=30.

We next investigated if metastatic growth in ZF model was regulated by EMT. RNAi was therefore employed to target the EMT transcriptional factors Snail and Zeb1 to block the EMT trait. In vitro, the knockdown of Snail1 significantly inhibited Vimentin expression but increased E-Cadherin Expression while the knockdown of Zeb1 only enhanced E-Cadherin expression without suppressing Vimentin (Fig. 5c). When both Snail kd and Zeb1 kd cells were respectively transplanted into ZF, total cancer burden at the metastatic site was significantly reduced at 6dpi comparing to SCR control (Fig. 5d), indicating that host microenvironment dependent acquisition of an EMT trait is essential for the metastatic tumor initiation in ZF.

Discussion

Bone metastasis of PCa is a multiple-steps process initiated by few disseminated cancer cells. In this research, we established a zebrafish xenograft model to monitor the metastatic behavior of PCa cells at a single cell resolution. We showed that human osteotropic, androgen independent PCa cells can extravasate, proliferate, and form perivescular metastases in 4-6 days. This metastatic behavior was associated with enhanced EMT and CSC traits in the cancer cells colonizing the zebrafish hematopoietic niche. Knockdown of Cripto, a Nodal co-receptor that was upregulated by ZF niche microenvironment in PCa metastasis, significantly inhibited metastatic tumorigenicity through suppression of EMT plasticity in ZF. In addition, targeting of EMT transcriptional factors in PCa cells prior engraftment also significantly suppressed metastatic growth at CHT.

Our results indicate that ZF microenvironment can induce human cancer cell plasticity. This cancer cell-microenvironment interaction in ZF resembles what happens in mammals [9, 10, 34]. In mice xenografts, human PCa cells can target the hematopoietic stem cell niche in bone marrow to establish a foothold inducing CSC enrichment. This CSC enrichment was partially regulated by osteoblasts [9, 34]. When PCa cells were co-cultured with osteoblasts in vitro, $ALDH^{hi}$ subpopulation was enriched accompanied by an elevated expression of Cripto and induction of EMT, leading to an aggressive phenotype of the cancer cells. Given that the response of the human PCa cells to ZF CHT signals was similar to the PCa cells response to osteoblasts, the molecular cues driving the Cripto expression and $ALDH^{hi}$ subpopulation enrichment in both conditions seems to be comparable.

Interaction between human cancer cells and ZF microenvironment was described before. CXCL-12, for instance, is an essential cytokines present in bone marrow leading to bone metastatic colonization of cancer cells [35]. In ZF, human cancer cells can sense host (ZF) CXCL-

12 which is produced by mesenchymal stem cells in CHT [32], inducing metastatic colonization [28, 29]. Targeting of either CXCR-4 (CXCL-12 receptor) in breast human cancer cells or CXCL-12 in ZF significantly inhibited extravasation and metastatic tumor growth at CHT area. In addition, ZF myeloid cells were shown to guide human cancer cell extravasation and invasion by reorganizing extracellular matrix at the metastatic site [27]. Taken together, those studies indicated a functional interaction between human cancer cells and zebrafish microenvironment leading to the metastatic phenotype. A combination of different platforms including ZF xenografts, osteoblasts co-culturing and mammalian xenografts can therefore be employed to study the molecular and cellular cues driving cancer cell plasticity.

In this research, we addressed how ZF microenvironment governs metastatic onset of PCa cells. It was previously reported that Cripto has an enhanced expression in PCa bone metastasis and correlates with poor prognosis in stratified high-risk patients [34, 36]. In PC-3M-Pro4, Cripto is upregulated in $ALDH^{hi}$ subpopulation in culture and is required for experimental metastasis in zebrafish and mice xenografts [34] Here, we showed that Cripto drives PCa cancer metastatic tumor initiation through induction of EMT at the metastatic onset.

The role of EMT in cancer progression is still under discussion [20]. It was originally recognized as a driver of cancer cell invasion and metastatic dissemination [37]. After seeding to the niche, the EMT-reversed program MET is still required to initiate tumor outgrowth [37, 38]. As evidence, metastatic tumor-initiating capacity was diminished after inducing sufficient, irreversible EMT by ectopic expression of EMT TFs, indicating the importance of MET in metastatic tumor outgrowth [38-40]. In contrast, other researches demonstrated that tumor initiation was associated with an occurrence of transient EMT, which endowed cancer cells with enhanced tumor-initiating capacity / CSC traits [18, 19]. In prostate cancer, it was suggested that the cells with EMT status harbors CSC traits while MET is associated with a more proliferative capacity [41]. Although this research proposed that the heterogenic cell population with different EMT/MET status may have distinctive functions in metastatic process, due to a limitation of animal models for real-time single cell tracking, they cannot directly monitor the dynamic of the cell states at the initial stage of metastatic tumor growth. Here, using ZF xenografts, we observed that both PC-3 and PC-3M-Pro4 obtained enhanced EMT and CSC traits after metastatic seeding. This transient EMT is essential for metastatic tumor initiation. Targeting of either Snail or Zeb1 to reverse EMT significantly inhibited metastatic tumorigenicity. To further elucidate how EMT-MET plasticity play roles in long term PCa metastatic tumor outgrowth as described by others, studies with PCa cell lines bearing EMT reporter and inducible EMT/MET TFs expression system can be performed using the immunodeficiency ZF xenograft model [25], which allows long-term single-cell tracking for human cancer cell metastasis.

Overall, in this study we employed a ZF xenograft model to track PCa cell plasticity at early stage of metastasis. We showed that the PCa cells at the metastatic site obtained enhanced

EMT and CSC traits which were partially controlled by the induction of Cripto. Targeting either Cripto or other EMT factors may therefore have a significant clinical potential. Moreover, our data highlight that ZF xenograft model can be applied as a powerful tool to study the role of cancer cell-microenvironment interaction in cancer stem- and EMT-plasticity regulation.

Acknowledgements

We thank Dr Gabriel van der Pluijm (Deportment of Urology, LUMC) for providing experimental material, Guido de Roo from the Flow cytometry facility (Department of Hematology, LUMC) for technical support, Prof. Rob Hoeben and Martijn Rabelink (Department of Cell Biology, LUMC) for providing lentiviral shRNA vectors (Sigma-Aldrich). The present work was supported by a personalized medicine grant from Alpe D'HuZes (AdH)/KWF PROPER entitled "Near-patient prostate cancer models for the assessment of disease prognosis and therapy" (UL2014-7058), SNF 31003A_169352 from Swiss National Science Foundation, FP7 GA 316125) from European Commission and a MAESTRO grant (2012/06/A/NZ1/0008) from National Science Center.

Reference

1. Jemal, A., et al., *Global patterns of cancer incidence and mortality rates and trends.* Cancer Epidemiol Biomarkers Prev, 2010. **19**(8): p. 1893-907.
2. Hanahan, D. and R.A. Weinberg, *Hallmarks of cancer: the next generation.* Cell, 2011. **144**(5): p. 646-74.
3. Lambert, A.W., D.R. Pattabiraman, and R.A. Weinberg, *Emerging Biological Principles of Metastasis.* Cell, 2017. **168**(4): p. 670-691.
4. Shibata, M. and M.M. Shen, *The roots of cancer: stem cells and the basis for tumor heterogeneity.* Bioessays, 2013. **35**(3): p. 253-60.
5. Germann, M., et al., *Stem-like cells with luminal progenitor phenotype survive castration in human prostate cancer.* Stem Cells, 2012. **30**(6): p. 1076-86.
6. Collins, A.T., et al., *Prospective identification of tumorigenic prostate cancer stem cells.* Cancer Res, 2005. **65**(23): p. 10946-51.
7. van den Hoogen, C., et al., *High aldehyde dehydrogenase activity identifies tumor-initiating and metastasis-initiating cells in human prostate cancer.* Cancer Res, 2010. **70**(12): p. 5163-73.
8. Chaffer, C.L., et al., *Poised Chromatin at the ZEB1 Promoter Enables Breast Cancer Cell Plasticity and Enhances Tumorigenicity.* Cell, 2013. **154**(1): p. 61-74.
9. Shiozawa, Y., et al., *Human prostate cancer metastases target the hematopoietic stem cell niche to establish footholds in mouse bone marrow.* Journal of Clinical Investigation, 2011. **121**(4): p. 1298-1312.
10. Shiozawa, Y., et al., *The marrow niche controls the cancer stem cell phenotype of disseminated prostate cancer (vol 7, pg 41217, 2016).* Oncotarget, 2017. **8**(23): p. 38075-38075.

11. Polyak, K. and R.A. Weinberg, *Transitions between epithelial and mesenchymal states: acquisition of malignant and stem cell traits.* Nature Reviews Cancer, 2009. **9**(4): p. 265-273.
12. Mani, S.A., et al., *The epithelial-mesenchymal transition generates cells with properties of stem cells.* Cell, 2008. **133**(4): p. 704-715.
13. Guo, W., et al., *Slug and Sox9 cooperatively determine the mammary stem cell state.* Cell, 2012. **148**(5): p. 1015-28.
14. Kalluri, R. and R.A. Weinberg, *The basics of epithelial-mesenchymal transition.* Journal of Clinical Investigation, 2009. **119**(6): p. 1420-1428.
15. Yang, J. and R.A. Weinberg, *Epithelial-mesenchymal transition: At the crossroads of development and tumor metastasis.* Developmental Cell, 2008. **14**(6): p. 818-829.
16. Viebahn, C., *Epithelio-mesenchymal transformation during formation of the mesoderm in the mammalian embryo.* Acta Anatomica, 1995. **154**(1): p. 79-97.
17. Shibue, T. and R.A. Weinberg, *EMT, CSCs, and drug resistance: the mechanistic link and clinical implications.* Nature Reviews Clinical Oncology, 2017. **14**(10): p. 611-629.
18. Tran, H.D., et al., *Transient SNAIL1 expression is necessary for metastatic competence in breast cancer.* Cancer Res, 2014. **74**(21): p. 6330-40.
19. Moody, S.E., et al., *The transcriptional repressor Snail promotes mammary tumor recurrence.* Cancer Cell, 2005. **8**(3): p. 197-209.
20. Thompson, E.W. and I. Haviv, *The social aspects of EMT-MET plasticity.* Nat Med, 2011. **17**(9): p. 1048-9.
21. Brabletz, T., *EMT and MET in metastasis: where are the cancer stem cells?* Cancer Cell, 2012. **22**(6): p. 699-701.
22. White, R., K. Rose, and L. Zon, *Zebrafish cancer: the state of the art and the path forward.* Nat Rev Cancer, 2013. **13**(9): p. 624-36.
23. Postlethwait, J.H., et al., *Vertebrate genome evolution and the zebrafish gene map.* Nat Genet, 1998. **18**(4): p. 345-9.
24. Dooley, K. and L.I. Zon, *Zebrafish: a model system for the study of human disease.* Curr Opin Genet Dev, 2000. **10**(3): p. 252-6.
25. Yan, C., et al., *Visualizing Engrafted Human Cancer and Therapy Responses in Immunodeficient Zebrafish.* Cell, 2019.
26. Letrado, P., et al., *Zebrafish: Speeding Up the Cancer Drug Discovery Process.* Cancer Res, 2018. **78**(21): p. 6048-6058.
27. He, S., et al., *Neutrophil-mediated experimental metastasis is enhanced by VEGFR inhibition in a zebrafish xenograft model.* J Pathol, 2012. **227**(4): p. 431-45.
28. Tulotta, C., et al., *Inhibition of signaling between human CXCR4 and zebrafish ligands by the small molecule IT1t impairs the formation of triple-negative breast cancer early metastases in a zebrafish xenograft model.* Dis Model Mech, 2016. **9**(2): p. 141-53.
29. Sacco, A., et al., *Cancer Cell Dissemination and Homing to the Bone Marrow in a Zebrafish Model.* Cancer Res, 2016. **76**(2): p. 463-71.
30. Lawson, N.D. and B.M. Weinstein, *In vivo imaging of embryonic vascular development using transgenic zebrafish.* Dev Biol, 2002. **248**(2): p. 307-18.
31. Chen, L., et al., *A zebrafish xenograft model for studying human cancer stem cells in distant metastasis and therapy response.* Methods Cell Biol, 2017. **138**: p. 471-496.
32. Tamplin, O.J., et al., *Hematopoietic stem cell arrival triggers dynamic remodeling of the perivascular niche.* Cell, 2015. **160**(1-2): p. 241-52.

33. Pettaway, C.A., et al., *Selection of highly metastatic variants of different human prostatic carcinomas using orthotopic implantation in nude mice.* Clin Cancer Res, 1996. **2**(9): p. 1627-36.
34. Zoni, E., et al., *CRIPTO and its signaling partner GRP78 drive the metastatic phenotype in human osteotropic prostate cancer.* Oncogene, 2017. **36**(33): p. 4739-4749.
35. Kucia, M., et al., *Trafficking of normal stem cells and metastasis of cancer stem cells involve similar mechanisms: pivotal role of the SDF-1-CXCR4 axis.* Stem Cells, 2005. **23**(7): p. 879-94.
36. Liu, Y., et al., *Cripto-1 promotes epithelial-mesenchymal transition in prostate cancer via Wnt/beta-catenin signaling.* Oncol Rep, 2017. **37**(3): p. 1521-1528.
37. Beerling, E., et al., *Plasticity between Epithelial and Mesenchymal States Unlinks EMT from Metastasis-Enhancing Stem Cell Capacity.* Cell Rep, 2016. **14**(10): p. 2281-8.
38. Celia-Terrassa, T., et al., *Epithelial-mesenchymal transition can suppress major attributes of human epithelial tumor-initiating cells.* J Clin Invest, 2012. **122**(5): p. 1849-68.
39. Tsai, J.H., et al., *Spatiotemporal Regulation of Epithelial-Mesenchymal Transition Is Essential for Squamous Cell Carcinoma Metastasis.* Cancer Cell, 2012. **22**(6): p. 725-736.
40. Ocana, O.H., et al., *Metastatic colonization requires the repression of the epithelial-mesenchymal transition inducer Prrx1.* Cancer Cell, 2012. **22**(6): p. 709-24.
41. Ruscetti, M., et al., *Tracking and Functional Characterization of Epithelial-Mesenchymal Transition and Mesenchymal Tumor Cells during Prostate Cancer Metastasis.* Cancer Res, 2015. **75**(13): p. 2749-59.